An Experimentally Validated Steady State Polymer Electrolyte Membrane Water Electrolyser Model

Ishanka Dedigama[1], Kathy Ayers[2], Paul R. Shearing[1] and Daniel J. L Brett[1,*]

[1]Electrochemical Innovation Lab, Department of Chemical Engineering, UCL, London, UK.
[2]Proton OnSite, Wallingford, USA.
[*]E-mail: d.brett@ucl.ac.uk

A simple electrochemical model is developed to understand the overpotentials associated with a polymer electrolyte membrane water electrolyser (PEMWE) operating at room temperature (20 °C) and atmospheric pressure (1 atm). The model is validated using experimental results and fitted parameter values are reported.

1. INTRODUCTION

For several decades, proton exchange membrane water electrolyser (PEMWE) technology was mainly used to produce oxygen for space and underwater applications. Currently it has renewed interest for the production of hydrogen using renewable energy sources [1, 2]. It has many advantages over the traditional alkaline water electrolysis systems, such as: higher operating current densities (> 1.5 A cm^{-2}) due to higher active surface areas and minimisation of inter-electrode spacing [3]; greater safety, as there is no caustic electrolyte circulated in the system; greater reliability, as less difficulties due to corrosion are encountered; simplified and more compact design [4-8]; and ability to generate compressed gasses directly as they can sustain higher differential pressures (up to 350 bar) [9].

However, there is scope for further development of this technology; reducing production costs to meet market requirements, increasing system efficiencies and improving manufacturing techniques. Therefore, in order to address these matters it is important to have a good understanding of the electrochemical properties and the behaviour of an electrolyser. Mathematical modelling is a useful tool in developing electrochemical technology such as PEMWEs.

Models have been developed that describe the current-potential characteristics of PEMWEs [10-12], determine control strategy [13, 14], understand the effect of operating performance [15, 16], analyse the integration with renewable energy sources [17] and demonstrate the effect of temperature [18]. Furthermore, electrical equivalent circuit models [19, 20] and thermal models have also been developed [17].

The current study presents a simple electrochemical model focusing on activation and ohmic overpotentials and is validated using experimental results obtained from a single cell PEMWE.

2. ELECTROCHEMICAL MODEL DEVELOPMENT

PEM electrolysis cell (PEMEC) modelling is a useful tool to understand the fundamental nature of device operation. A model not only provides a framework to analyse the characteristics of current and voltage of an electrolyser but it also supplies the values of internal variables which are difficult to measure, such as the exchange current densities.

A simple steady-state model is developed for an unpressurised PEMWE based on mass balances, transport and electrochemical kinetics of a PEMWE that represents the relationship between the operating voltage of the cell and the current.
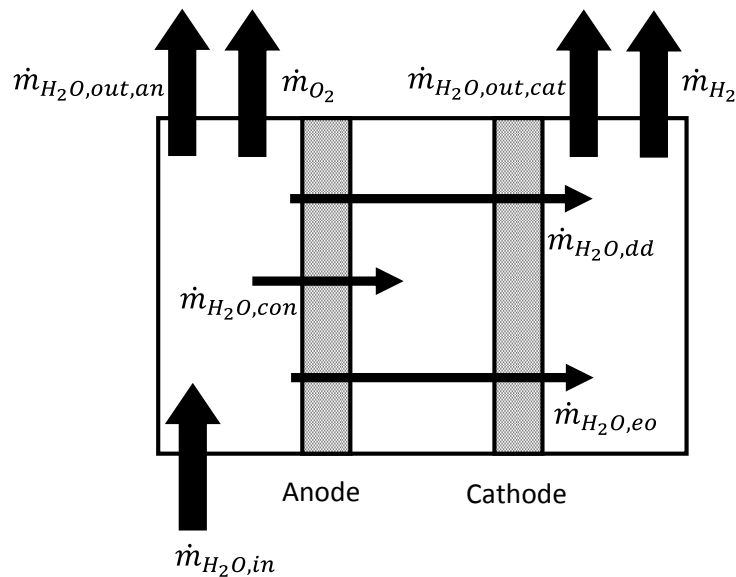
2.1. Assumptions

The model presented here is based on the following simplifying assumptions: steady state conditions; constant temperature (20 °C) and pressure (atmospheric pressure, 1 atm); ideal gases; 100% Faradaic efficiency, fully hydrated membrane; no cross-over of gases. The current (I) across the cell is assumed to be uniformly distributed:

$$I = iA \qquad (1)$$

where i is the current density and A is the active area.

2.2. Mass Balance

The mass balance over a controlled volume can be expressed using the mass flow rates ($\dot{m}$) of the feed water and the products, hydrogen and oxygen. Figure 1 illustrates the mass flow in a PEMWE, where $\dot{m}_{H_2O,in}$, $\dot{m}_{H_2O,out,an}$ and $\dot{m}_{H_2O,out,cat}$ are the inlet and outlet mass flow rates of water at the anode and the outlet mass flow rate of water at the cathode respectively. $\dot{m}_{H_2}$ and $\dot{m}_{O_2}$ are the mass flow rates of hydrogen and oxygen produced at the cathode and the anode. $\dot{m}_{H_2O,dd}$ and $\dot{m}_{H_2O,eo}$ are mass flow rate of water flowing from the anode to the cathode due to the concentration gradient and the electro-osmotic drag. $\dot{m}_{H_2O,cons}$ is the mass flow rate of water consumed by the electrochemical reaction split into hydrogen and oxygen.

Figure 1. Illustration summarising mass flow inside a PEMEC.

The formal definition for material balances from mass conservation in a system can be written as:

$$Input + Generation - Output - Consumption = Accumulation \qquad (2)$$

Therefore, a simple mass balance can be performed, as described below.

2.2.1. Anode chamber

As shown in Figure 1, the water coming out from the anode chamber is the difference between the water fed at the anode, water being consumed to produce oxygen and the amount of water that flows through the membrane:

$$\dot{m}_{H_2O,out,an} = \dot{m}_{H_2O,in} - \dot{m}_{H_2O,m} - \dot{m}_{H_2O,cons} \qquad (3)$$

where $\dot{m}_{H_2O,m}$ is the mass flow rate of water through the membrane.

2.2.2. Cathode chamber

The amount of water flowing out from the cathode chamber is equal to the amount that flows through the membrane, as water is not consumed at the cathode.

$$\dot{m}_{H_2O,out,cat} = \dot{m}_{H_2O,m} \qquad (4)$$

The water flux through the membrane is governed by three mechanisms: electro-osmotic drag from the anode to cathode, diffusion driven by concentration gradient from the anode to cathode and convection if a pressure gradient is present [21]. In this study, convection in not considered as the pressure is assumed to be at a constant value of 1 atm at the anode and the cathode. The direction of water flux across the membrane is shown in Figure 1 and can be written as [22]:

$$\dot{m}_{H_2O,m} = \dot{m}_{H_2O,dd} + \dot{m}_{H_2O,eo} \tag{5}$$

Molar flow rate of species i can be related to its mass flow rate as:

$$\dot{N}_i = \frac{\dot{m}_i}{mw_i} \tag{6}$$

where $\dot{N}_i$ is the molar flow rate of component i and mw_i is the molecular weight of component i.

The molar flow rates of the hydrogen and oxygen produced and the water consumed can be related to the current applied to the cell by Faraday's law:

$$\dot{N}_{H_2} = \frac{I}{2F}, \quad \dot{n}_{H_2} = \frac{i}{2F} \tag{7}$$

$$\dot{N}_{O_2} = \frac{I}{4F}, \quad \dot{n}_{O_2} = \frac{i}{4F} \tag{8}$$

$$\dot{N}_{H_2O,cons} = \frac{I}{2F}, \quad \dot{n}_{H_2O,cons} = \frac{i}{2F} \tag{9}$$

where $\dot{n}$ is the molar flux, I is the current, i is the current density and F is Faraday constant (96485 C mol^{-1}).

2.2.3. Diffusion transport

The water diffusion through the membrane is due to the concentration gradient of water across the membrane that favours the water flow from the anode to the cathode as the anode is constantly flooded due to fluent water from the pump. A large concentration gradient can be expected when the electrolyser starts operation as the cathode side is initially dry. The diffusion transport can be evaluated by the following equation [23]:

$$\dot{N}_{H_2O,dd} = \frac{AD_{eff}}{\delta_m} \left(C_{H_2O,an} - C_{H_2O,cat} \right) \tag{10}$$

where D_{eff} is the effective water diffusion coefficient in the membrane, δ_m is the membrane thickness and $C_{H_2O,an}$ and $C_{H_2O,cat}$ represent the water concentrations at the two sides of the membrane.

The effective diffusion coefficient for water transport inside the gas diffusion layer (GDL) and the membrane can be expressed using the Bruggeman equation [20, 24, 25]:

$$D_{eff} = \varepsilon^{1.5} D_w \tag{11}$$

where D_w is the diffusion coefficient of water and can be evaluated to have a value of 1.28×10^{-10} m^2 s^{-1} through expressions reported by Springer *et al.* [26], and ε is the porosity of the electrode. A commonly used value of $\varepsilon = 0.3$ is employed here [27].
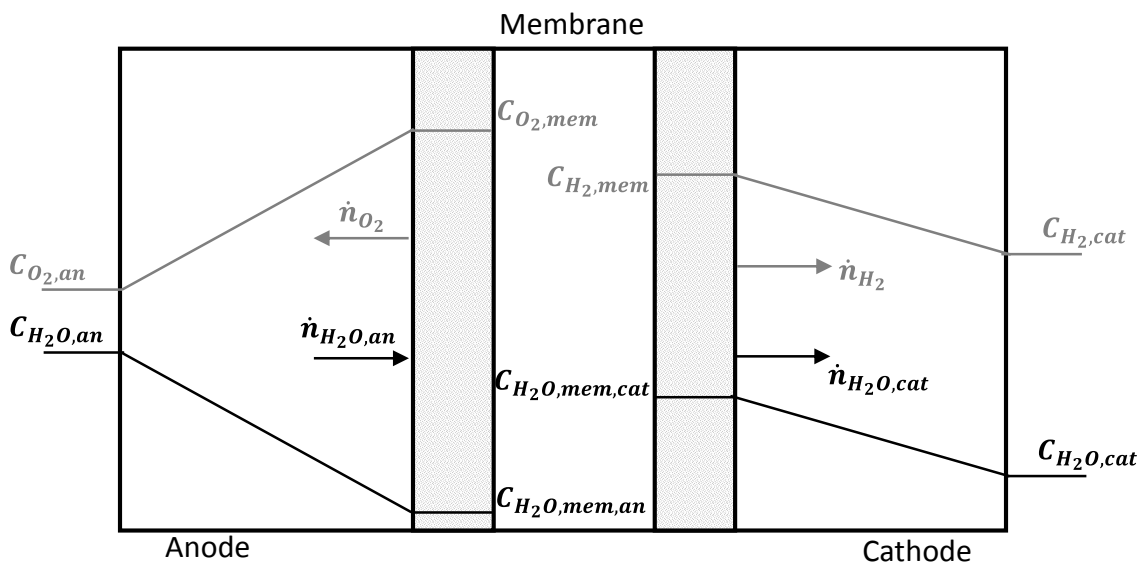
Figure 2. Species concentration inside a PEMEC.

The concentration gradient of water between the electrodes is the driving force in diffusion through the membrane and is illustrated in Figure 2. The concentration of water on either side of the membrane can be expressed as a function of water content as shown in the following expressions [28]:

$$C_{H_2O,an} = \frac{\rho_{m,dry}}{M_{m,dry}} \lambda_{an}, \quad C_{H_2O,cat} = \frac{\rho_{m,dry}}{M_{m,dry}} \lambda_{cat} \tag{12}$$

where $\rho_{m,dry}$ is the density of the dry membrane, $M_{m,dry}$ is the equivalent weight of a dry membrane and λ_{an} and λ_{cat} represent the water content on both sides of the membrane. The following expression has been formulated based on studies performed by Zawodzinski et al. [29] for the water content of a Nafion 117 membrane [26, 28]:

$$\lambda = 0.043 + 17.81a - 39.85a^2 + 36a^3, 0 < a \leq 1 \tag{13}$$

Where a is the activity of water and can be obtained using the following expression:

$$\alpha = x_{H_2O} \frac{P}{P_{sat}} \tag{14}$$

Where P is the local pressure, P_{sat} is the saturation pressure of water and x_{H_2O} is the mole fraction of water given by:

$$x_{H_2O,an} = \frac{n_{H_2O,an}}{n_{H_2O,an} + n_{O_2}}, \quad x_{H_2O,cat} = \frac{n_{H_2O,cat}}{n_{H_2O,cat} + n_{H_2}} \tag{15}$$

The activity of water at the anode is assumed to have a value of unity as water is present in bulk compared to the amount of oxygen being produced.

2.2.4. Electro-osmotic drag

The transport of water from the anode electrode domain to the cathode electrode domain due to the flux of hydrated protons migrating between the electrodes is known as the electro-osmotic drag. Hence, the molar flow can be expressed as [16, 30, 31]:

$$\dot{N}_{H_2O,eo} = n_d \frac{I}{F} \tag{16}$$

where n_d is the electro-osmotic drag coefficient $\left[mol_{H_2O} / mol_{H^+} \right]$.

There are a number of expressions presented in literature to find the electro-osmotic drag coefficient. Onda *et al*. [32] has reported that the electro-osmotic drag coefficient of a membrane electrode assembly (MEA) fabricated using electroplating is only dependent on the operating temperature (T) as expressed below:

$$n_d = 0.03 + 0.0134T$$
(17)

Work done by Ge *et al*. [33] reports that n_d is enhanced by the water content of the membrane and can be expressed as below when the water content of a PEM electrolyser is at a maximum due to the high water content at the anode.

$$n_d = 0.011 + 0.1949\lambda - 0.0139\lambda^2 + 4.060 \times 10^{-4}\lambda^3, \lambda \leq 1.40 \tag{18}$$

2.3. Open Circuit Voltage

The open circuit voltage (OCV) can be calculated from the Nernst equation, as follows [14, 34]:

$$E = E^0 + \frac{RT}{2F} \ln \frac{P_{H_2} P_{O_2}^{1/2}}{a_{H_2O}} \tag{19}$$

where, P_{H_2} and P_{O_2} are partial pressures of hydrogen and oxygen, R is the universal gas constant (8.314 J mol^{-1} K^{-1}) and E^0 is the equilibrium cell voltage at standard temperature and pressure and can be related to the Gibbs free energy, ΔG of the electrochemical reaction as shown in Equation (20):

$$E^0 = -\frac{\Delta G}{2F} \tag{20}$$

Furthermore, the expression derived by LeRoy and Bowen [35] can be used to determine the OCV at atmospheric pressure:

$$E = 1.5184 - 1.5421 \times 10^{-3}T + 9.523 \times 10^{-5}T\ln(T) + 9.84 \times 10^{-8}T^2 \tag{21}$$

However, the practical cell voltage of a PEMEC is higher than the OCV. This difference is caused by the voltage drops that occur across a cell due to activation, diffusion (mass transport) and ohmic overpotentials (losses). Therefore, the real cell voltage can be written as:

$$E_{cell} = E + \eta_{act} + \eta_{dd} + \eta_{ohm} \tag{22}$$

where η_{act} is the activation overpotential, η_{dd} is the diffusion overpotential and η_{ohm} is the ohmic overpotential.

2.4. Activation Overpotential

Activation overpotential represents the electrochemical kinetic behaviour; hence it is a representation of the speed of the reactions taking place at the electrode surface. Therefore, a portion of the voltage applied is lost in transferring the electrons to or from the electrodes. This activation loss (η_{act}) can be deduced from the Butler-Volmer equation [36]:

$$i = i_0 \left[exp\left(\frac{\alpha_{an} nF}{RT} \eta_{act}\right) - exp\left(\frac{-\alpha_{cat} nF}{RT} \eta_{act}\right) \right] \tag{23}$$

where i_0 is the exchange current density, n is the number of electrons transferred and α_{an} and α_{cat} are the charge transfer coefficients for the anodic and cathodic processes.

The charge transfer coefficient is governed by the electron transfer occurring across the electrode-electrolyte interface. Equations (24) and (25) can be used to determine the anode and cathode charge transfer coefficient of a process where the reaction mechanisms are known [37].

$$\alpha_{an} = \frac{n-\gamma}{v} - s\beta \qquad (24)$$

$$\alpha_{cat} = \frac{\gamma}{v} + s\beta \qquad (25)$$

where n is the total number of electrons transferred in the overall reaction, γ is the number of electrons transferred before the rate determining step (rds), v is the number of times the rds occurs for one act of the overall reaction, s is the number of electrons transferred in the rds and β is the symmetry factor.

They can be simplified for a PEM system as follows [38]:

$$\alpha_{an} = (1-\beta)s \qquad (26)$$

$$\alpha_{cat} = \beta s \qquad (27)$$

Symmetric factor is the fraction of potential energy applied to a system that changes the reaction rate. For simplicity, this factor is commonly assumed to be 0.5 [38]. However, values ranging from 0.3 to 0.6 have been obtained from experimental data presented in literature [37]. Values between 0 to 2 have been used for α_{an} and 0 to 1 for α_{cat} in literature [38, 39].

For a system where the activation loss is large ($\eta_{act} >$ 200 mV), the Butler-Volmer equation can be simplified to Equation (28) [37]:

$$\eta_{act} = \frac{RT}{\alpha F} ln\left(\frac{i}{i_0}\right) \qquad (28)$$

Hence, the activation overvoltage at the anode and the cathode can be written as:

$$\eta_{act} = \frac{RT}{\alpha_{an}F} ln\left(\frac{i}{i_{0,an}}\right) \qquad (29)$$

$$\eta_{act} = \frac{RT}{\alpha_{cat}F} ln\left(\frac{i}{i_{0,cat}}\right) \qquad (30)$$

The exchange current density values have a substantial effect on the activation overpotential and are greatly dependant on the materials and porosity of the electrodes; concentration, distribution and dimensions of the catalyst particles and operating temperature [40]. The exchange current density can be calculated from an Arrhenius-type relation:

$$i_0 = Ae^{-E_{act}/RT} \qquad (31)$$

where A is the pre-exponential factor and E_{act} is the activation energy.

Typically, $i_{0,an}$ and $i_{0,cat}$ vary between $10^{-3} – 10^{-12}$ A cm^{-2} and $0.2 – 10^{-3}$ A cm^{-2} respectively [17, 38, 41-44]. However Biaku *et al.* [18] has published $i_{0,cat} = 0.287$ A cm^{-2} and $i_{0,an} = 1.0 \times 10^{-6}$ A cm^{-2} as experimental cathode and anode exchange current density values at 20 °C for a HOGEN-40 electrolyser manufactured by Proton Energy Systems.

2.5. Diffusion Overvoltage

Diffusion overvoltage, also known as the concentration overpotential, occurs due to the change in concentration of the reactants at the electrode surfaces when electrolysis is in progress.

In a PEM electrolysis system, as the electrochemical reaction takes place, water needs to be supplied to the electrode-membrane interface, whereas hydrogen and oxygen should be removed from it. Therefore, the mass flows are transported through the porous electrode according to the diffusion phenomena described by Fick's law. If the oxygen and hydrogen produced in an electrolysis system are not removed as fast as they are being produced, there will be an increase due to mass transport limitations. This diffusion overvoltage can be estimated using the Nernst equation, as shown below [16, 36]:

$$\eta_{dd} = E_1 - E_0 = \left(E^0 + \frac{RT}{nF} \ln C_1\right) - \left(E^0 + \frac{RT}{nF} \ln C_0\right) = \frac{RT}{nF} \ln \frac{C_1}{C_0} \qquad (32)$$

where n is the number of electrons transferred during the reaction and '0' is a working condition taken as reference.

Hence, Equation (32) can be applied to find the diffusion overvoltage at both the anode and the cathode:

$$\eta_{dd,an} = \frac{RT}{4F} \ln \frac{C_{O_2,mem}}{C_{O_2,0}} \qquad (33)$$

$$\eta_{dd,cat} = \frac{RT}{2F} \ln \frac{C_{H_2,mem}}{C_{H_2,0}} \qquad (34)$$

where $C_{O_2,mem}$ and $C_{H_2,mem}$ represent oxygen and the hydrogen concentrations at the membrane electrode interface, respectively.

Diffusion overvoltage occurs when the current is high enough to hinder the reaction by overpopulating the membrane surface with oxygen gas bubbles and hence slowing down the reaction rate [18]. However, diffusion overvoltage is assumed to be negligible as this work focuses on PEM electrolysers operating at moderate current densities (up to 1 A cm^{-2}).

2.6. Ohmic Overvoltage

The ohmic overvoltage is caused by the resistance to the flow of electrons by the electrolyte, the electrodes and their various interconnectors. Ohmic overvoltage is linearly proportional to the current and can be expressed as:

$$\eta_{ohm} = R_{cell}I \tag{35}$$

where R_{cell} is the ohmic resistance of the cell.

The magnitude of the ohmic resistance is a combination of the resistances opposed by the electrodes, the plates, and the membrane and can be written as:

$$\eta_{ohm} = \left(R_{an} + R_{cat} + R_p + R_m\right)I = \left(R_e + R_p + R_m\right)I$$
$$\eta_{ohm} = \eta_{ohm,e} + \eta_{ohm,p} + \eta_{ohm,m} \tag{36}$$

where R_{an}, R_{cat}, R_p and R_m are resistances of the anode, cathode, bipolar plates and the membrane, and $\eta_{ohm,e}$, $\eta_{ohm,p}$ and $\eta_{ohm,m}$ are the ohmic overpotentials caused by the electrodes, bipolar plates and the membrane respectively.

2.6.1. Electrodes and Plates

The voltage losses associated with electron transfer through the electrode and the flow field plate are found by adopting the electric circuit analogy presented by Marr and Li [25] shown in Figure 3. Applying ohms law on the electrode and the flow field plate gives:

$$R = \rho_{eff}\frac{\iota}{A} \tag{37}$$

where ι is the length of the electrons path, A is the cross-section of the conductor and ρ_{eff} is the effective resistivity of the electrode which is given by:

$$\rho_{eff} = \frac{\rho_{bulk}}{(1-\varepsilon)^{3/2}} \tag{38}$$

It is assumed that the total average path length of an electron is $(w_c + w_s)/4$, where w_c and w_s are the width of a channel and channel support respectively. Therefore, the average resistance in the electrode per half flow channel becomes [25]:

$$R_1 = \frac{\rho_{eff}(w_c+w_s)}{4\delta_e L} \tag{39}$$

where δ_e and L are the thickness and the length of the electrode. If the number of channels in the flow field plate is n_{ch} then the total resistance of the electrode becomes:

$$R_e = \frac{\rho_{eff}(w_c + w_s)}{8n_{ch}\delta_e L} \tag{40}$$

R_2 denoted in Figure 3 indicates the resistance caused by the right portion of the flow field plate that is given by:

$$R_2 = \frac{\rho_p h_p}{wL} \tag{41}$$

where ρ_p is the resistivity of the current collection plate, h_p is the distance from the outside border of the plate to the channel surface, W is the width and L is the length of the plate. Similarly, the resistance of each channel support is:

$$R_s = \frac{\rho_p h_c}{w_s L} \tag{42}$$

where h_c is the height of the channel. Considering there are $n_{ch} + 1$ channel supports, the total resistance of the flow-field plate becomes:

$$R_p = \frac{R_s}{n_{ch}+1} + R_2 \tag{43}$$
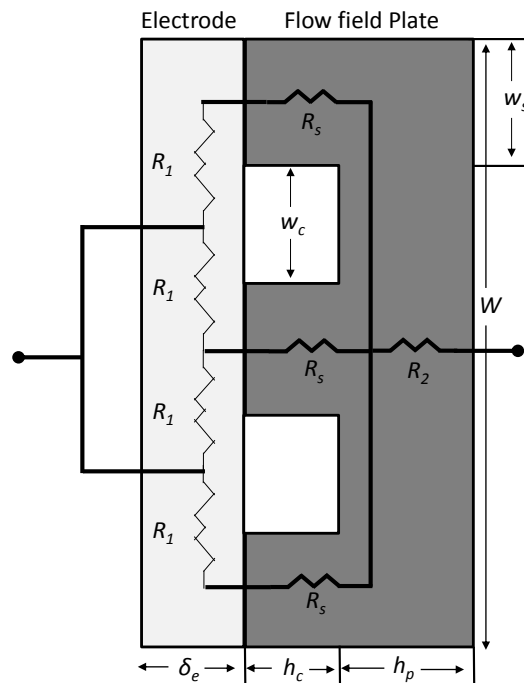
Figure 3. Electrical circuit representation of the resistances of the plates and the electrode in a PEMWE.

2.6.2. Membrane

Membrane

The dominant losses in η_{ohm} are the ionic losses caused by resistance to the ion flow through the membrane. This resistance caused by the membrane can be expressed as shown in Equation (44):

$$\eta_{ohm,m} = \frac{\delta_m}{\sigma_m} i \qquad (44)$$

Where σ_m and δ_m are the conductivity and the thickness of the membrane.

A study by Ito *et al*. [45] compares different analysis present in literature on proton conductivity of Nafion membranes. The expression (Equation 45) suggested by Springer *et al*. [26] provides conductivity in terms of water content and the temperature of the membrane. The expression suggested by Bernardi and Verbrugge [24] (Equation 46) gives conductivity as a function of protonic diffusion coefficient and concentration in the membrane and is used in this model. Further studies done by Radev *et al*. [46] suggest a value of 0.094 S cm^{-1} for the proton conductivity of a Nafion 117 membrane at 80 °C and 100% relative humidity.

$$\sigma_m = (0.005139\lambda - 0.00326)exp\left[1268\left(\frac{1}{303} - \frac{1}{T}\right)\right] \qquad (45)$$

$$\sigma_m = \frac{F^2 C_{H^+} D_{H^+}}{RT} \qquad (46)$$

where λ and T are the water content and temperature of the membrane and C_{H^+} and D_{H^+} are the concentration of H^+ ions and protonic diffusion coefficient in the membrane.

3. MODEL IMPLIMENTATION

Table 1. Physical properties of the PEMWE.

Membrane	Nafion 117
Anode/Cathode electrode	Platinum
Anode GDL	Platinum coated titanium porous sheet and a mesh
Cathode GDL	Toray carbon paper
Anode flow field plate	Titanium - parallel flow
Cathode flow field plate	Graphite - triple serpentine

The model is developed for a PEMWE cell assembled with key components listed in Table 1 and operating at room temperature (20 °C) and atmospheric pressure (1 atm) and assuming mass transport limitations are negligible in the current density range considered. The physical parameters of the electrolysis cell are listed in Table 2.

The developed model was implemented in MATLAB along with estimated parameter values listed in Table 3 to obtain a theoretical V-I curve for the electrolyser. The accuracy of the model is established by comparing it with experimental voltage-current data for a PEMWE operating under identical conditions.

Table 2. Physical parameters of the PEMWE cell.

|	
Temperature, T	293 K
Pressure, P	1.0 atm
Membrane active area, A	2.5×10^3 mm^2
Membrane thickness, δ_m	0.178 mm
Anode Thickness, δ_{an}	5.0×10^{-2} mm
Cathode thickness, δ_{cat}	5.0×10^{-2} mm
Length of the electrode, L	50 mm
Width of the electrode, W	50 mm
Width of anode channel, $w_{c,an}$	2.5 mm
Width of cathode channel, $w_{c,cat}$	1.0 mm
Width of anode support, $w_{s,an}$	3.6 mm
Width of cathode support, $w_{s,cat}$	1.0 mm
Distance from anode plate edge to the channel surface, $h_{p,an}$	12 mm
Distance from cathode plate edge to the channel surface, $h_{p,cat}$	11.7 mm
Anode channel height, $h_{c,an}$	3.0 mm
Cathode channel height, $h_{c,cat}$	1.0 mm
Number of anode channels, $n_{ch,an}$	9
Number of cathode channels, $n_{ch,cat}$	30
Number of anode supports, $n_{s,an}$	8
Number of cathode supports, $n_{s,cat}$	30

Table 3. Estimated parameter values

Parameter	Value	Unit	Reference
Anode charge transfer coefficient, α_{an}	0.1		[36]
Cathode charge transfer coefficient, α_{cat}	0.9		[36]
Water diffusion coefficient, D_w	1.28×10^{-10}	$m^2\,s^{-1}$	[26]
Porosity of the electrodes, ε	0.3		[27]
Anode exchange current density, $i_{0,an}$	1×10^{-6}	$A\,cm^{-2}$	[17, 38, 41-44]
Cathode exchange current density, $i_{0,cat}$	0.29	$A\,cm^{-2}$	[18]
Hydrogen concentration, C_{H^+}	1200	$mol\,m^{-3}$	[24]
Diffusivity of hydrogen, D_{H^+}	4.5×10^{-9}	$m^2\,s^{-1}$	[24]
Electrode resistivity, ρ_{bulk}	9.85×10^{-8}	$\Omega\,m$	[47]
Anode resistivity, ρ_{an}	47.8×10^{-8}	$\Omega\,m$	[48]
Cathode resistivity, ρ_{cat}	16.0×10^{-6}	$\Omega\,m$	[49]
Saturated water vapor pressure P_{sat}	0.467	atm	[24]
Equivalent weight of dry membrane, $M_{m,dry}$	1.1	$kg\,mol^{-1}$	[20, 50]
Density of dry membrane, $\rho_{m,dry}$	2000	$kg\,m^{-3}$	[20, 50]

4. EXPERIMENTAL

4.1. PEMWE setup and electrochemical measurements

Electrochemical measurements were made on a 25 cm^2 cell (Fuel Cell Technologies, USA) that was made up of a Ti current collection plate with a single channel flow-field and a graphite cathode bipolar plate with a triple serpentine flow-field with integrated Pt reference electrode, as shown in Figure 4. The MEA was provided by Proton OnSite, CT, USA and comprised a Nafion 117 membrane and a 40–60 μm thick layer of Pt catalyst on either side. The anode GDL was platinised porous Ti and carbon paper was used as the cathode GDL.

Anode and total cell polarisation measurements were made on the cell by performing linear galvanostatic sweep using an Iviumsts.XRi high-current potentiostat, with Iviumboost, (Alvatek Ltd, UK). The current was swept from 0 to 15 A (0 – 0.6 A cm^{-2}) at room temperature (20 °C) and pressure (1 atm).
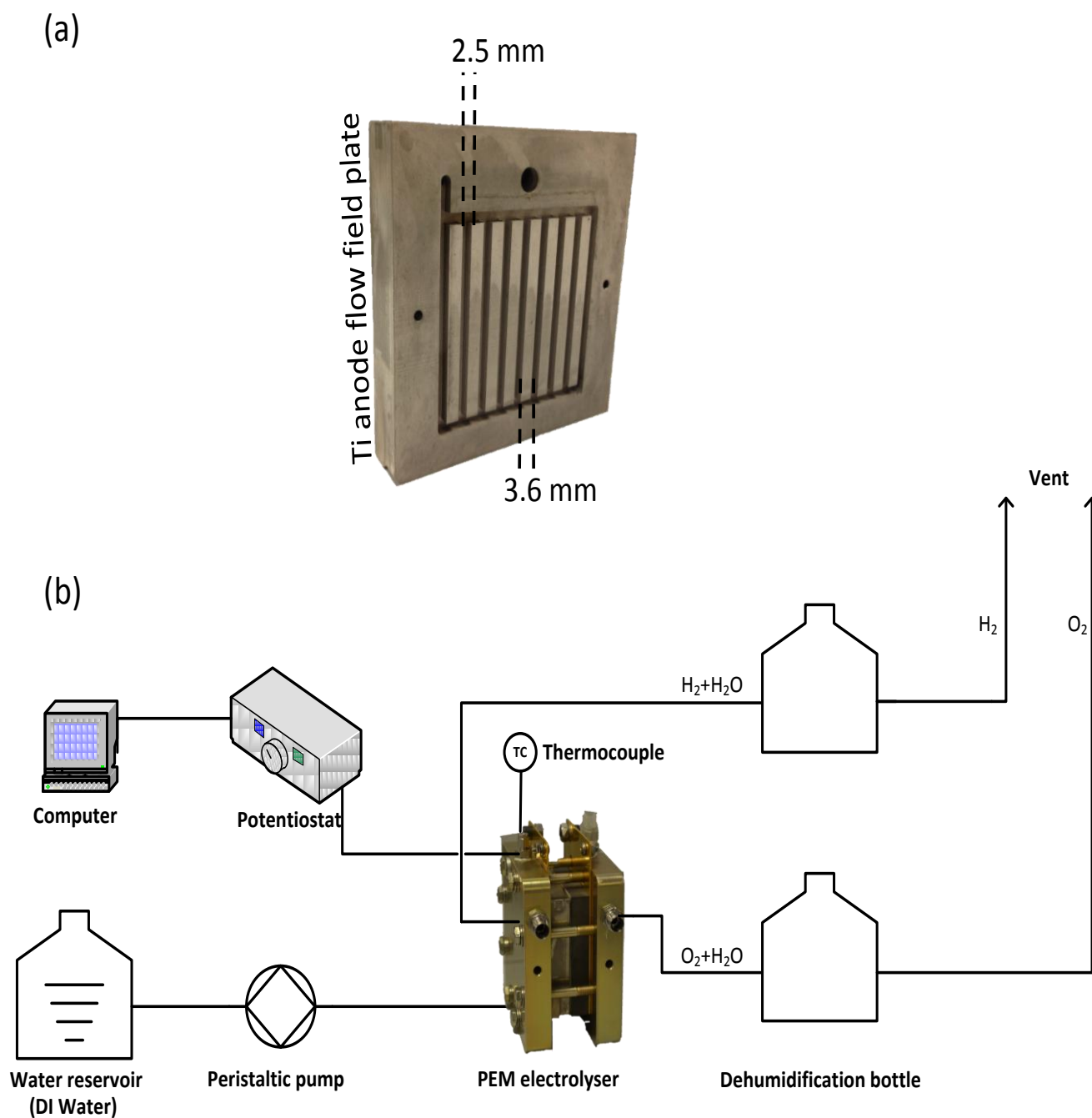
Figure 4. (a) The configuration of the anode flow field plate; (b) PEMWE electrolyser cell used for experimental studies and the experimental set-up.

5. MODEL VALIDATION AND PARAMETER ESTIMATION

Experimental and theoretical anode polarisation results are shown in Figure 5. It shows that the model fits well with the experimental data obtained for the anode.
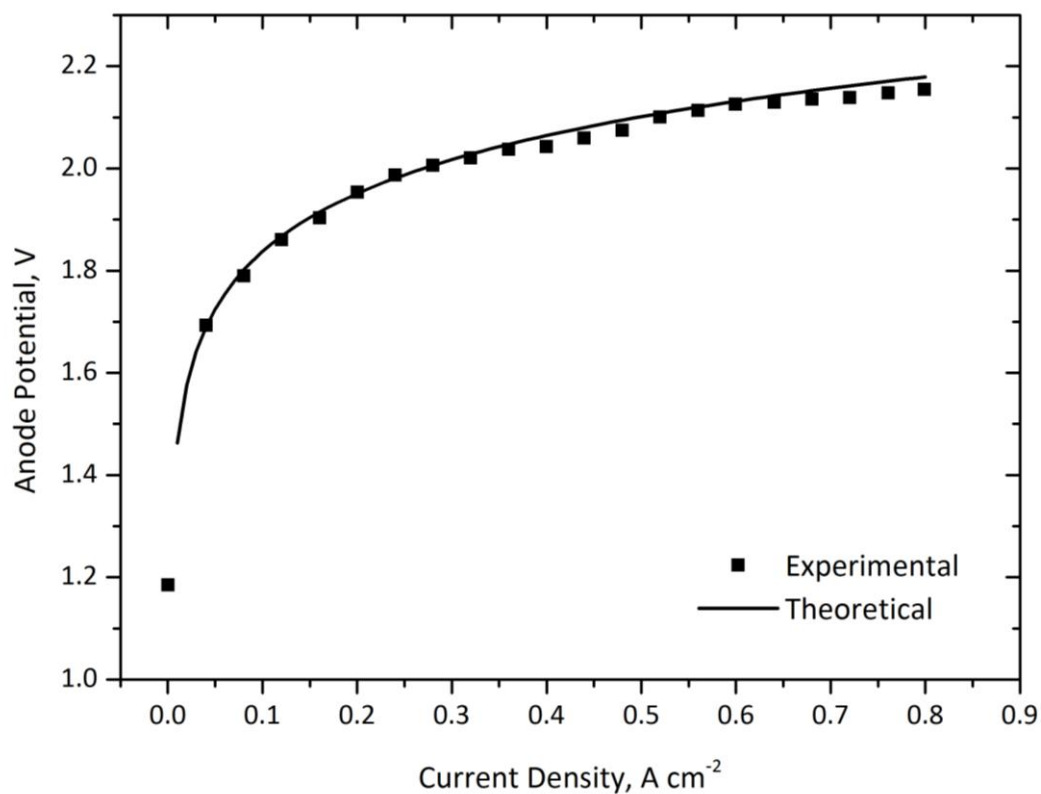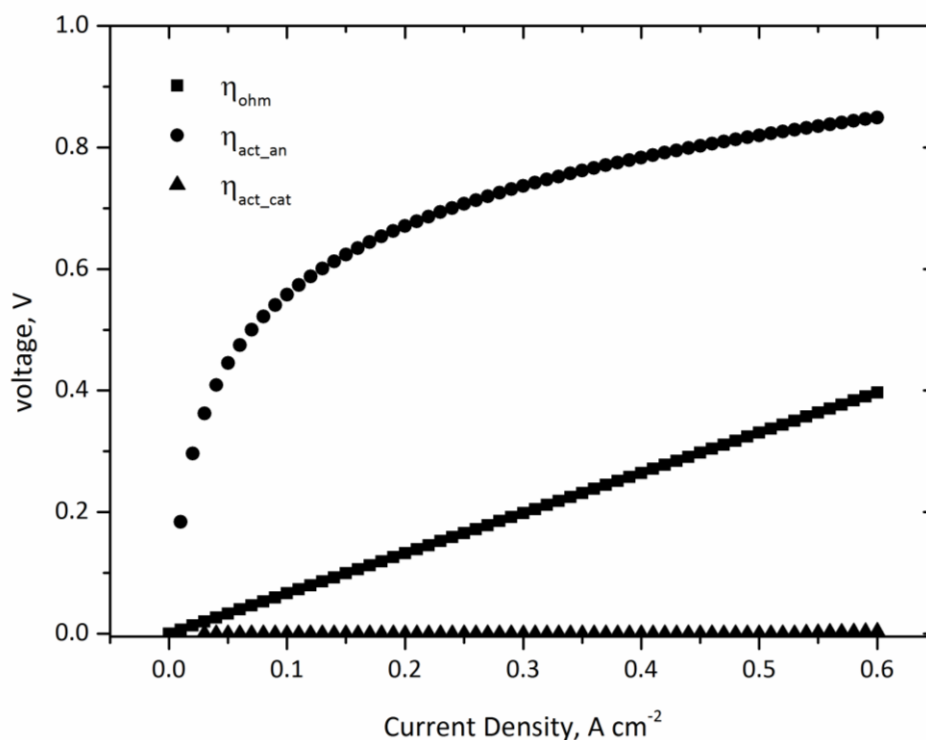
Figure 5. Comparison of the experimental and theoretical anode polarisation of PEMWE operating at room temperature (20 °C) and atmospheric pressure.
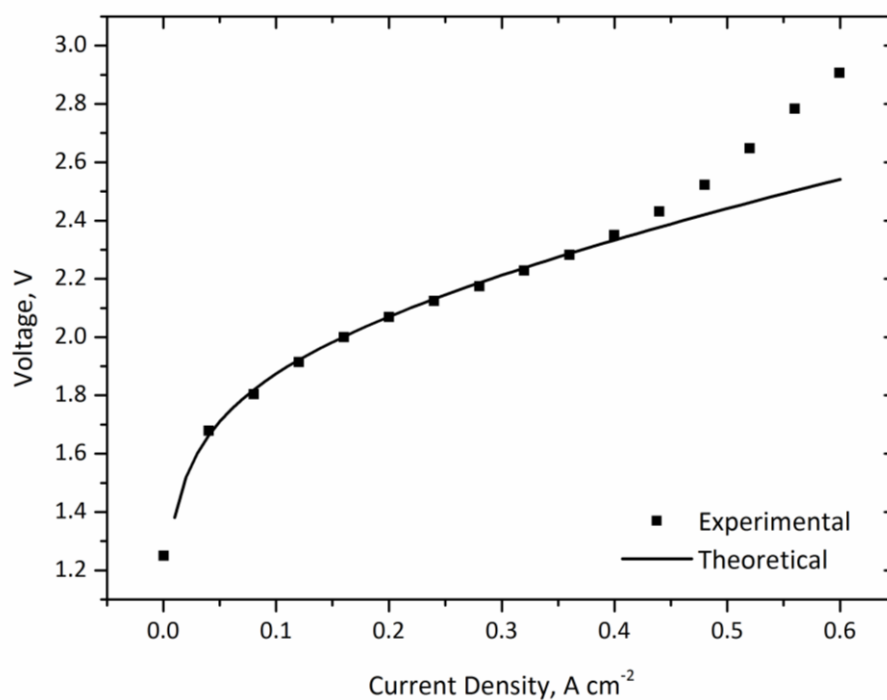
Figure 6. Comparison of theoretical and experimental for a PEMWE operating at room temperature (20 °C), atmospheric pressure and water flow rate of 1 ml min^{-1}.

Figure 7. Contribution of anode and cathode activation overpotentials and ohmic overpotential towards the operating potential of a PEMWE cell.

Figure 6 presents a comparison between the experimental and theoretical polarisation data obtained for the PEMWE under identical conditions. It can be seen that the model developed agrees well with the experimental data, supporting the validity of the model. However, it can be noticed that the experimental data begins to deviate from the model as the current density increases (at about 0.5 A cm^{-2}) due to mass transport limitations that are neglected in this model. Figure 7 shows the contribution of each overpotential towards the overall performance of the cell. The ohmic overpotential increases linearly with current density. The cathode overpotential is relatively small due to fast kinetics of HER and the cell potential is dominated by anode activation overpotential due its slow kinetics. It should be noted that a relatively high anode activation overpotential is observed as a non-optimised Pt-Pt electrode is used in these experiments.

A sensitivity analysis carried out on the estimated parameters of the electrolysis cell exhibited that the anode exchange current density has the largest influence on the cell potential. It also showed that the model was sensitive to charge transfer coefficients, cathode exchange current density and water diffusivity. The model can be expressed as Equation (43) and was fitted to experimental voltage-current data using the Non-linear Least Square (NLS) method to obtain values for the estimated parameters. In fitting the data, care was taken to ensure non-negative values for all parameters, parameters were only allowed to be within the range of those previously reported in the literature and ensuring $i > i_{0,cat}$ for the Tafel equation to be valid.

$$V = E_0 + \frac{RT}{F}\left(arcsinh\left(\frac{i}{2i_{0,an}}\right)\right) + \frac{RT}{F}\left(arcsinh\left(\frac{i}{2i_{0,cat}}\right)\right) + (R_e + R_p)Ai + \frac{\delta_m RT}{F^2 C_{H^+} D_{H^+}} i \qquad (47)$$

Statistical comparison was made between the mathematical model and the experimental data in order to evaluate the accuracy of the mathematical model. It can be seen that the fit obtained for experimental data shows a good match with the model, as the goodness of fit (R^2) is 0.98 and the sum of squares due to errors (SSE) and the root mean squared error (RMSE) have values of 4.35×10^{-2} and 6.59×10^{-2} respectively.

Table 4 compares the numerical values used in the mathematical model with the experimental values. Furthermore, electrochemical impedance spectroscopy (EIS) measurements carried out previously on the cell gave an ohmic resistance of 0.058 Ω cm^2 [51], which corresponds to a D_{H^+} value of 5.0×10^{-10} m^2 s^{-1}, which is similar to the fitted value of 6.0×10^{-10} m^2 s^{-1}.

Table 4. Initial estimated and fitted parameter values of the PEMWE**.**

Parameter	α_{an}	α_{cat}	$i_{0,an}$ (A cm^{-2})	$i_{0,cat}$ (A cm^{-2})	D^+_H (m^2 s^{-1})
Estimated	0.1	0.9	3.50×10^{-3}	0.29	1.0×10^{-9}
Fitted	0.079	0.921	3.24×10^{-3}	0.50	6.0×10^{-10}

6. CONCLUSION

The electrochemical model developed gives insight into the various overpotentials influencing PEMWE operation under ambient conditions. Activation and ohmic overpotentials are dominant under low current density operation and the anode activation overpotential governs the operating potential of the cell under operating conditions considered in this study. Validation of the model was carried out with experimental data obtained from a lab-scale PEMWE and the fitted parameter values are reported that are within the range of those published in literature.   Deviation of the model from experiment for the whole cell can be used as an indicator of the onset of mass transport limiting behaviour.

References

1. P. Millet, D. Dragoe, S. Grigoriev, V. Fateev and C. Etievant, *International Journal of Hydrogen Energy*, 34 (2009) 4974.

2. J. F. McElroy. *Journal of Power Sources*. 47 (1994) 369.
3. P. W. T. Lu and S. Srinivasan, *Journal of Applied Electrochemistry*, 9 (1979) 269.
4. P. Millet, F. Andolfatto and R. Durand. *International Journal of Hydrogen Energy*, 21 (1996) 87.
5. D. Labou, E. Slavcheva, U. Schnakenberg and S. Neophytides, *Journal of Power Sources*, 185 (2008) 1073.
6. S. A. Grigoriev, V. I. Porembsky and V. N. Fateev, *International Journal of Hydrogen Energy*, 31, (2006) 171.
7. G. Doucet, C. Etiévant, C. Puyenchet, S. Grigoriev and P. Millet. *International Journal of Hydrogen Energy*, 34 (2009) 4983.
8. P. Millet, T. Alleau and R. Durand. *Journal of Applied Electrochemistry*, 23 (1993) 322.
9. K. E. Ayers, E. B. Anderson, C. Capuano, B. Carter, L. Dalton, G. Hanlon, et al.. *ECS Transactions*, 33 (2010) 3.
10. P. Choi, D. G. Bessarabov and R. Datta. *Solid State Ionics*, 175 (2004) 535.
11. M. Ni, M. K. H. Leung, and D. Y. C. Leung. Electrochemistry modelling of Proton Exchange Membrane (PEM) water electrolysis for hydrogen production. WHEC. Lyon France (2006).
12. B. Laoun, M. Belhamel, W. Naceur and L. Serir. *Revue des Energies Renouvelables*. 11 (2008) 267.
13. H. Görgün. *International Journal of Hydrogen Energy*, 31 (2006) 29.
14. M. E Lebbal and S. Lecœuche. *International Journal of Hydrogen Energy*, 34 (2009) 5992.
15. M. Santarelli, P. Medina and M. Calì. *International Journal of Hydrogen Energy*, 34 (2009) 2519.
16. F. Marangio, M. Santarelli and M. Calì. *International Journal of Hydrogen Energy*, 34 (2009) 1143.
17. R. García-Valverde, N. Espinosa and A. Urbina. *International Journal of Hydrogen Energy*, 37 (2012) 1927.
18. C. Y. Biaku, N. V. Dale, M. D. Mann, H. Salehfar, A. J. Peters and T. Han. *International Journal of Hydrogen Energy*, 33 (2008) 4247.
19. O. Atlam and M. Kolhe. *Energy Conversion and Management*, 52 (2011) 2952.
20. P. Medina and M. Santarelli. *International Journal of Hydrogen Energy*, 35 (2010) 5173.
21. T. Berning, D. M. Lu and N. Djilali. *Journal of Power Sources*, 106 (2002) 284.
22. S. Grigoriev, A. Kalinnikov, P. Millet, V. Porembsky and V. Fateev. *Journal of Applied Electrochemistry*, 40 (2010) 921.
23. R. B. Bird, W. E. Stewart and E. N. Lightfoot *Transport Phenomena*. second edition ed. John Wiley & Sons, New York (2007).
24. D. M. Bernardi and M. W. Verbrugge. *AIChE Journal*, 37 (1991) 1151.
25. C. Marr and X. Li. *ARI - An International Journal for Physical and Engineering Sciences*. 50 (1998) 190.
26. T. E. Springer, T. A. Zawodzinski and S. Gottesfeld, *Journal of Electrochemical Society*. 138 (1991) 2334.
27. J. C. Amphlett, R. M. Baumert, R. F. Mann, B. A. Peppley, P. R. Roberge and T. J. Harris. *Journal of The Electrochemical Society*, 142 (1995) 1.
28. S. Shimpalee and J. W. Van Zee. *International Journal of Hydrogen Energy*, 32 (2007) 842.
29. T. A. Zawodzinski, C. Derouin, S. Radzinski, R. J. Sherman, V. T. Smith, T. E. Springer, et al. *Journal of The Electrochemical Society*. 140 (1993) 1041.
30. T. Tschinder, T. Schaffer, S. Fraser and V. Hacker, *Journal of Applied Electrochemistry*, 37 (2007) 711.
31. X. Li, S. Qu, H. Yu, M. Hou, Z. Shao and B. Yi, *Journal of Power Sources*, 190 (2009) 534.
32. K. Onda, T. Murakami, T. Hikosaka, M. Kobayashi, R. Notu and K. Ito, *Journal of The Electrochemical Society*, 149 (2002) A1069.
33. S. Ge, B. Yi and P. Ming. *Journal of The Electrochemical Society*, 153 (2006) A1443.

34. M. H. Nehrir and C. Wang. *Modeling and control of fuel cells*, John Wiley & Sons, New Jersey (2009).
35. R. L. LeRoy, C. T. Bowen and D. J. LeRoy. *Journal of The Electrochemical Society*, 127 (1980) 1954.
36. J. Larminie and A. Dicks. *Fuel Cell Systems Explained* (2nd Edition). John Wiley & Sons, New Jersey (2003).
37. D. A. Noren and M. A. Hoffman. *Journal of Power Sources*, 152 (2005) 175.
38. M. G. Santarelli, M. F. Torchio and P. Cochis. *Journal of Power Sources*, 159 (2006) 824.
39. W. Frank. *A first course in electrochemical engineering*. Alfresford Press Ltd., England (1993).
40. M. G. Santarelli and M. F. Torchio. *Energy Conversion and Management*, 48, 2007, 40.
41. C. Song, Y. Tang, J. L. Zhang, J. Zhang, H. Wang, J. Shen, et al. *Electrochimica Acta.*, 52 (2007) 2552.
42. A. Parthasarathy, S. Srinivasan, A. J. Appleby and C. R. Martin, *Journal of The Electrochemical Society*, 139 (1992) 2530.
43. P. D. Beattie, V. I. Basura and S. Holdcroft, *Journal of Electroanalytical Chemistry*. 468 (1999) 180.
44. A. Damjanovic, A. Dey and J. O. M. Bockris. *Journal of The Electrochemical Society*, 113 (1966) 739.
45. H. Ito, T. Maeda, A. Nakano and H. Takenaka, *International Journal of Hydrogen Energy*, 36 (2011) 10527.
46. I. Radev, G. Georgiev, V. Sinigersky and E. Slavcheva. *International Journal of Hydrogen Energy*, 33 (2008) 4849.
47. R. W. Powell and R. P. Tye. *Platinum Metals Review*, 6 (1962) 138.
48. J. T. Milck. *Electrical resistivity data and bibliography on titanium and titanium alloys*. Airforce Materials Laboratory, Springfield (1970).
49. A. Goetz and A Holser, *Transactions of The Electrochemical Society*, 82 (1942) 391.
50. A. J. del Real, A. Arce and C Bordons, *Journal of Power Sources*, 173 (2007) 310.
51. I. Dedigama, T. J. Mason, J. Millichamp, K. Ayers, P. R. Shearing and D. J. L. Brett. An Electrochemical Impedance Spectroscopy Study of a Polymer Electrolyte Membrane Water Electrolyser. International Journal of Hydrogen Energy, submitted.